nanomaterials

MDPI

Article

On Capacitance and Energy Storage of Supercapacitor with Dielectric Constant Discontinuity

Shiqi Zhou

School of Physics and Electronics, Central South University, Changsha 410083, China; chixiayzsq@163.com

Abstract: The classical density functional theory (CDFT) is applied to investigate influences of electrode dielectric constant on specific differential capacitance C_d and specific energy storage E of a cylindrical electrode pore electrical double layer. Throughout all calculations the electrode dielectric constant varies from 5, corresponding to a dielectric electrode, to $\varepsilon_{wr} = 10^8$ corresponding to a metal electrode. Main findings are summarized as below. (i): By using a far smaller value of the solution relative dielectric constant $\varepsilon_r = 10$, which matches with the reality of extremely narrow tube, one discloses that a rather high saturation voltage is needed to attain the saturation energy storage in the ultra-small pore. (ii): Use of a realistic low $\varepsilon_r = 10$ value brings two obvious effects. First, influence of bulk electrolyte concentration on the C_d is rather small except when the electrode potential is around the zero charge potential; influence on the E curve is almost unobservable. Second, there remain the C_d and E enhancing effects caused by counter-ion valency rise, but strength of the effects reduces greatly with dropping of the ε_r value; in contrast, the C_d and E reducing effects coming from the counter-ion size enhancing remain significant enough for the low ε_r value. (iii) A large value of electrode relative dielectric constant ε_r^w always reduces both the capacitance and energy storage; moreover, the effect of the ε_r^w value gets eventually unobservable for small enough pore when the ε_r^w value is beyond the scope corresponding to dielectric electrode. It is analyzed that the above effects take their rise in the repulsion and attraction on the counter-ions and co-ions caused by the electrode bound charges and a strengthened inter-counter-ion electrostatic repulsion originated in the low ε_r value.

Keywords: ultra-small pore supercapacitor; dielectric discontinuity; differential capacitance; energy storage

check for updates

Citation: Zhou, S. On Capacitance and Energy Storage of Supercapacitor with Dielectric Constant Discontinuity. *Nanomaterials* **2022**, *12*, 2534. https://doi.org/10.3390/nano12152534

Academic Editor: Fabrizio Pirri

Received: 15 June 2022
Accepted: 22 July 2022
Published: 23 July 2022

Publisher's Note: MDPI stays neutral with regard to jurisdictional claims in published maps and institutional affiliations.

Copyright: © 2022 by the author. Licensee MDPI, Basel, Switzerland. This article is an open access article distributed under the terms and conditions of the Creative Commons Attribution (CC BY) license (https://creativecommons.org/licenses/by/4.0/).

1. Introduction

In the vicinity of a charged electrode, electrolyte solution forms an electric double layer (EDL) that reflects the competition between electrostatic attraction of the counter-ions to the electrode surface and the translational entropy of the ions. The EDL is a problem of fundamental importance to subjects as diverse as colloid science [1,2], macromolecular conformation [3,4], and biological membranes [5], and has been a subject of much research interest over the past several decades [6–11]. It is well known that charged colloids (i.e., macroions) have typically a low relative dielectric constant ($\varepsilon_r \approx 2-5$) which is much smaller than that of the surrounding solvent (e.g., for water $\varepsilon_r \approx 80$). In most of the simulation and theoretical works [12–18], it is generally assumed that the electrolyte solution and electrode have the same relative dielectric constant.

Usually, the electrode is a metal whose relative dielectric constant is infinite. In this case, the resultant induced charges (caused by the electric field excited by ions in the EDL) on the electrode surface result in an additional electrostatic force on the ions. The electrolyte ions in the EDL excites electric field, which causes a redistribution of the free electrons in the metal; finally, the distribution of the induced charges and salt ions reaches an equilibrium state under the action of the total electric field generated by the induced charges and electrolyte ions. At the same time, the electrostatic potential distribution over the electrode and the EDL region is also determined. If other dielectrics are mixed in the electrode

material [19,20] (in order to produce an electrode with a low relative dielectric constant), the bound charge generated by the dielectric due to the polarization of the electric field will also participate in the above process. As for the problem what is the primary electrostatic force on the ions in the solutions, this depends on the ratio of dielectric material to metal material constituting the electrode and the resulting average relative dielectric constant. The lower the electrode relative dielectric constant, the more the bound charges play a major role. From fundamental electrostatics the standard treatment of surface polarization at a dielectric boundary is through imaginary image charges in the medium of the electrode and consequent image forces. Surface polarization forces radically influence the ion distribution and hence, the mean electrostatic potential and surface force [21–24].

Understanding the surface polarization effect can increase our ability to control the EDL structure and disclose work mechanisms for many practical applications, such as the design of a supercapacitor (SC) [25–28], modulating three-dimensional conformation of polyelectrolyte brush [29], self-assembly [30,31], ionic profiles [22,23,32], and surface force [21,33–39].

The present work aims to consider a dielectric discontinuity of the electrode interface in the classical density functional theory (CDFT) framework. The dielectric discontinuity denotes two phases with different dielectric constants in contact; at the phase boundary, the dielectric constant changes discontinuously. The other two quality indicators of the dielectric, dielectric loss and dielectric strength, are not considered, because these characteristics are completely beyond interpretation scope of the CDFT, and they are suitable to be considered by other theories or molecular dynamics simulations [40]. As in the usual electrolyte theories or simulations, we use a general dielectric constant without considering the dependence on temperature and frequency. The CDFT is a convenient starting point for the microscopic structure and thermodynamic properties of inhomogeneous fluids [41,42]. It successfully accounts for the correlation and repulsive volume effects, and is widely applied to many fields of classical statistical mechanics, such as adsorption [43–46], phase transitions [47–54], inter-surface effective interactions [55–58], electrical double layer [6,59–63], polymer statistics [64–66], and solid [67–69].

The dielectric discontinuity CDFT is then applied to investigate influence of the electrode dielectric constant on differential capacitance and energy storage of the EDL inside a cylindrical pore. In the present work, the electrolyte solution is modeled by the primitive model (PM), and the solution relative dielectric constant ε_r is kept fixed at 10.0, this value is far smaller than that of bulk water. This is another novel point of the present work as a considerable part of the works for the SC [16,70–73] employing aqueous electrolyte solution uses the ε_r value corresponding to that of the bulk water. This is necessary because as the device size becomes smaller and smaller, amount of solvent adsorption near the interface tends to decrease [74]; moreover, correlation of the electric dipole perpendicular to the surface also decreases. It is the two factors [75] that leads to a decrease of the aqueous dielectric constant inside the pore.

Innovation of this work is that the classical density functional theory is applied to dielectric discontinuity for the first time. In an earlier work [76], it was clearly written: "However, the density functional theory and the field theoretic approach have not been applied to the case of the polarized electrode".

Layout of the paper is structured as follows. The CDFT approach considering the dielectric discontinuity is briefly presented in Section 2; model calculations for influences of the electrode dielectric constant at low bulk dielectric constant value are performed and the relevant results are presented and discussed in Section 3; finally, the main conclusions are summarized in Section 4.

2. Model and Method

In the present work, we consider the EDL formed by aqueous electrolyte confined by a cylindrical pore electrode. The pore is infinitely long, and its radius is R. The cylindrical pore wall (i.e., the electrode) is hard and perfectly smooth with dielectric constant $\varepsilon_1 = \varepsilon_0\varepsilon_r^w$,

where ε_0, ε_r^w are vacuum dielectric constant and electrode relative dielectric constant, respectively. The inner is charged with uniform surface charge area density σ. The model is briefly sketched in Figure 1. The aqueous electrolyte is modeled by the so-called PM. In the PM ions are considered as hard spheres (HS) of a diameter $d_{\pm}$. A point electric charge $Z_i e$ is placed at center of the HS. Z_i is the ion charge number (or ion valence) and e is the elementary charge strength. The solvent is mimicked by a continuous dielectric medium of dielectric constant $\varepsilon_2 = \varepsilon_0 \varepsilon_r$ (ε_r is relative dielectric constant contributed by the solvent).

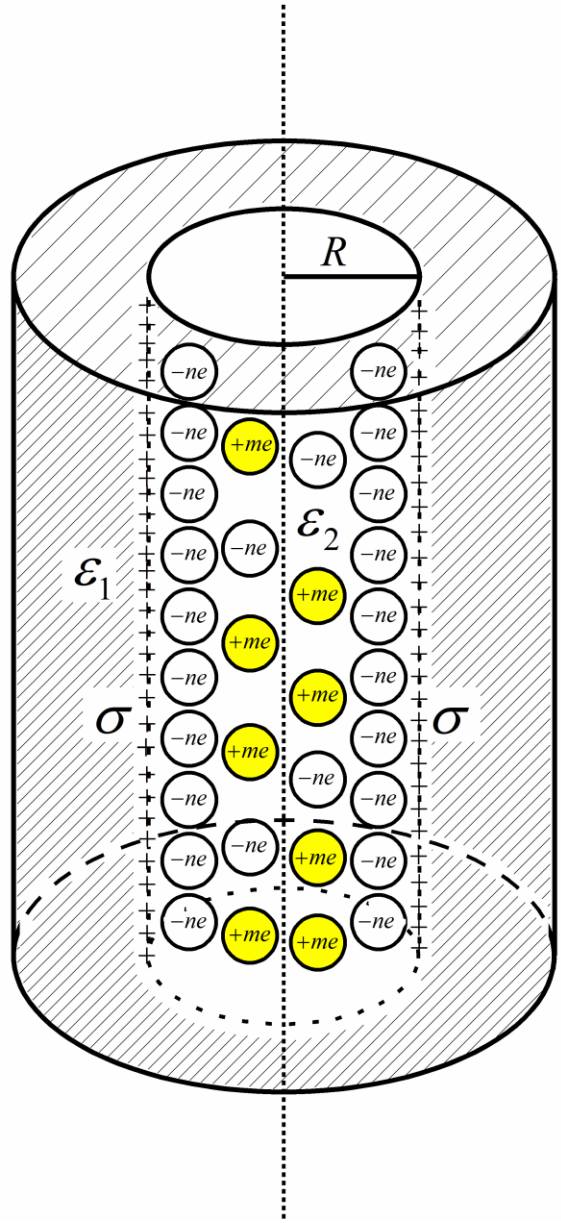

Figure 1. Diagram of the model considered. The electrical double layer is formed by $+m/-n$ (cation and anion electric valences are, respectively, $+m$ and $-n$) PM electrolyte inside an infinitely long cylindrical pore of radius R and with uniformly distributed charges on the inner surface of area charge strength σ. The electrolyte fluid is with medium dielectric constant ε_2, and the electrode has dielectric constant ε_1.

It is usually convenient to describe polarization of the interface by introducing image charges. For spatially confined systems with curved interfaces or for two closely located plane interfaces (for thin interlayers), an accurate description of polarization requires the

introduction of an infinite series of image charges. To deal with the dielectric discontinuity for a generic interface, it is necessary to numerically solve the corresponding boundary value problem for the Poisson equation. Although this is usually too time consuming to be feasible in simulations, it does not constitute any computational burden in the CDFT calculations.

The electrostatic potential distribution $\psi(\mathbf{r})$ satisfies the Poisson equation in uniform area V_i with dielectric constant ε_i ($i = 1, 2$):

$$\nabla^2\psi_i(\mathbf{r}) = -\frac{\rho(\mathbf{r})}{\varepsilon_i} \tag{1}$$

where $\rho(\mathbf{r})$ is the free charge density in V_i which is contributed by mobile electrolyte ions. There are two uniform areas for the present model: V_1 denotes the electrode, V_2 denotes the EDL inside the cylindrical electrode pore. At the electrode surface facing the EDL, the electrostatic potential distribution is continuous, i.e.,

$$\psi_1(\mathbf{r}) = \psi_2(\mathbf{r}) \tag{2}$$

The potential derivative satisfies another boundary value relation:

$$\varepsilon_2\frac{\partial\psi_2(\mathbf{r})}{\partial n} - \varepsilon_1\frac{\partial\psi_1(\mathbf{r})}{\partial n} = -\sigma \tag{3}$$

$\frac{\partial}{\partial n}$ denotes the partial derivative along normal direction, pointing from V_1 to V_2. σ denotes the free charge area density on the interface between V_1 and V_2, i.e., the electrode surface charge area density. For metal electrode with $\varepsilon_r^w = \infty$, because the metal electrode in the state of electrostatic balance is an equipotential body, Equation (3) reduces to:

$$\varepsilon_2\frac{\partial\psi_2(\mathbf{r})}{\partial n} = -\sigma \tag{4}$$

By inserting the infinite value of the relative dielectric constant into Equation (1), one infers immediately that within the metal electrode the electric field strength $\vec{E}$ satisfies the following equation:

$$\nabla \cdot \vec{E} = 0 \tag{5}$$

According to integral transformation, one has:

$$\oint_S \vec{E} \cdot d\vec{S} = \int_V \nabla \cdot \vec{E} dV = 0 \tag{6}$$

which, combined with the Gauss theorem, gives that there is no free charge inside the electrode hole. Obviously, this is consistent with the electrostatic equilibrium properties of conductor.

The free charge density $\rho(\mathbf{r})$ is determined by the ion density distribution $\rho_i(\mathbf{r})$ in the EDL:

$$\rho(\mathbf{r}) = \sum_{i=1}^{2} \rho_i(\mathbf{r}) Z_i e \tag{7}$$

The summation runs over all ion species. The density distribution $\rho_i(\mathbf{r})$ is calculated by minimizing the grand potential $\Omega[\{\rho_i\}]$. In the CDFT, the $\Omega[\{\rho_i\}]$ is supposed to be a functional of $\rho_i(\mathbf{r})$, and is related to the intrinsic Helmholtz free energy $F[\{\rho_i\}]$ via the Legendre transform

$$\Omega[\{\rho_i\}] = F[\{\rho_i\}] + \sum_i \int d\mathbf{r}\rho_i(\mathbf{r})(u_{wi}(\mathbf{r}) - \mu_i) \tag{8}$$

where μ_i is chemical potential for the i type ion, and $u_{wi}(\mathbf{r})$ is an external potential acting on the i type species, and for the homogeneously charged and hard cylindrical pore surface of the present consideration, it is calculated as follows:

$$u_{\mathrm{wi}}(r) = \begin{cases} \infty, & r > R - d_i/2 \\ Z_i e \psi_{\mathrm{w}}, & r < R - d_i/2 \end{cases} \tag{9}$$

where ψ_{w} is the electrostatic potential generated by the electrode surface charge area density σ, and does not depend on r because of the columnar symmetry of the electrode charge distribution. The value of ψ_{w} is not trivial because it influences the density distribution $\rho_i(\mathbf{r})$ in the EDL; the value can be determined by the electrical neutral condition.

The intrinsic Helmholtz energy $F[\{\rho_i\}]$ includes the ideal gas contribution and the excess contribution F_{ex}. The former is analytically available from textbook of statistical thermodynamics, and the latter originates from internal interactions within the system, and its acquirement has to resort to approximations. In the present calculations, we use the density functional approximations tested in literatures [77–80]. In detail, the hard sphere repulsion coming from the internal inter-ion short-range interaction is treated by a well confirmed fundamental measure functional, the long-range inter-ion electrostatic interaction is dealt with by mean field approximation, and the interplay between the hard sphere repulsion and electrostatic interaction is calculated by a second order functional perturbation expansion whose expansion coefficient is exactly the bulk second order direct correlation function based on a mean spherical approximation closure to the Ornstein-Zernike integral equation. Relevant details are recorded in literatures [77–80] and not repeated here. Particularly, literature [80] indicates that the electrical capacitance properties of extreme nanoscale SC can still be predicted rather reliably even the prediction of density distribution becomes worse under the extreme condition.

After numerical solution of the Poisson equation and minimization of the grand potential $\Omega[\{\rho_i\}]$, both the density distribution and electrostatic potential distribution profiles in equilibrium are available. The differential capacitance per unit area C_d is calculated according to definition:

$$C_d = \frac{\partial \sigma}{\partial \psi_2(R)} \tag{10}$$

where, $\psi_2(R)$ is the electrode potential, which is defined with reference to potential of a bulk electrolyte.

Accordingly, the energy stored per unit area is calculated as:

$$E(U) = \int_0^U U_s C_d(U_s) dU_s \tag{11}$$

where the U is the final electrode potential, whereas the above $\psi_2(R)$ is only used to calculate the C_d value. So, the $\psi_2(R)$ value can be any value between zero and U.

3. Results and Discussion

Four different values of the electrode relative dielectric constant ε_r^w are used, namely, $\varepsilon_r^w = 5$, 500, 2000, and 10^8, respectively, among which, $\varepsilon_r^w = 10^8$ corresponds to a metal electrode, $\varepsilon_r^w = 5$ denotes a dielectric electrode. The ion diameters considered are around $d = 4 \times 10^{-10}$ m, so we use d as the length unit to non-dimensionalize the cation and anion diameters d_+ and d_-, respectively: the relevant reduced diameters are $d_+^* = d_+/d$ and $d_-^* = d_-/d$; the electrode surface charge area density σ is reduced as $\sigma^* = \sigma d^2/e$ (e is elementary charge strength); both counter-ion and co-ion adsorptions $\Gamma_{counter-ion}$ and Γ_{co-ion} are reduced as $\Gamma^*_{counter-ion} = \Gamma_{counter-ion} d^2$ and $\Gamma^*_{co-ion} = \Gamma_{co-ion} d^2$, respectively. Four values are considered for the reduced pore radius $R^* = R/d$: 2.5, 4.5, 5.5, and 7.5. $+m$:$-n$ type electrolyte is considered, several representative values are chosen for the relevant bulk mole concentration $c_{m:n}$: *125 M,1 M,2,5 M,4 M*. The thermodynamic

temperature and electrolyte relative dielectric constant ε_r are fixed at 298.15 K and 10, respectively. For clarity and comparison, we summarize the parameter combinations corresponding to each of Figures 2–6 in Table 1.

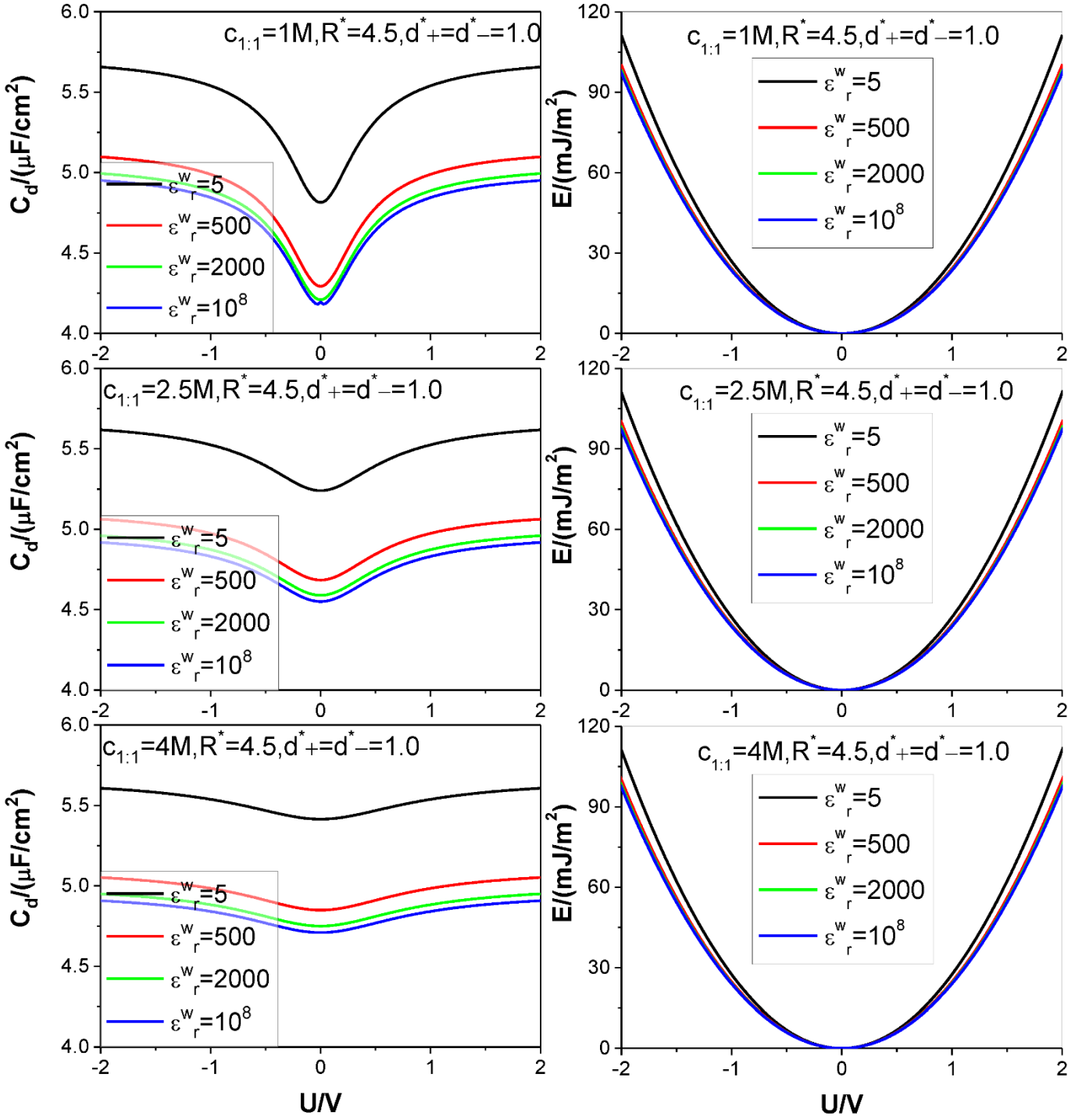

Figure 2. Curves of specific differential capacitance C_d and specific energy storage density E. Three values of bulk +1:−1 salt mole concentration and four values of the electrode relative dielectric constant ε_r^w are considered, as marked in the figures. Values of other parameters are marked in the text and figures, respectively.

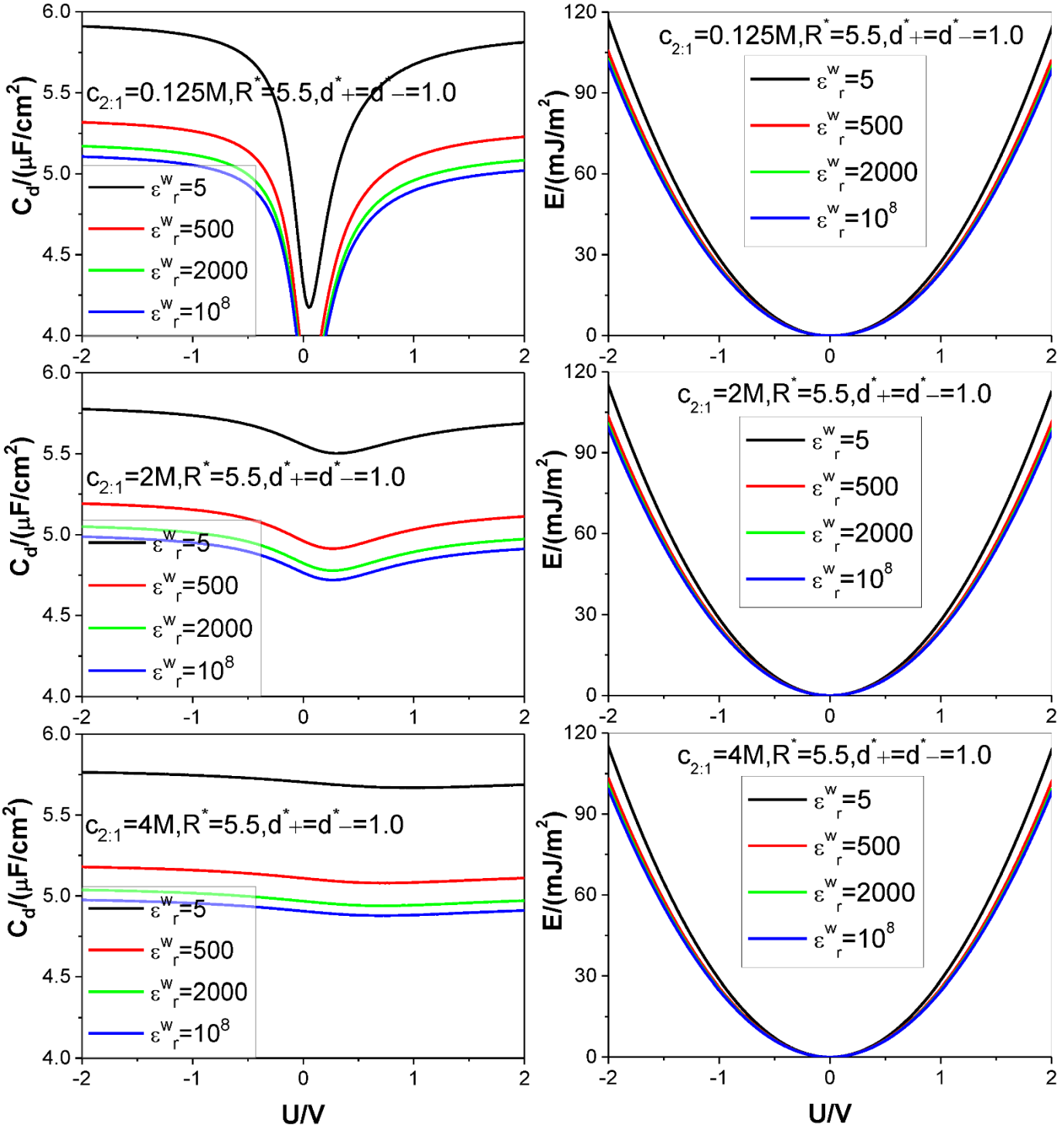

Figure 3. Same as in Figure 2 except that +2:−1 salt is considered. Values of other parameters are marked in the text and figures, respectively.

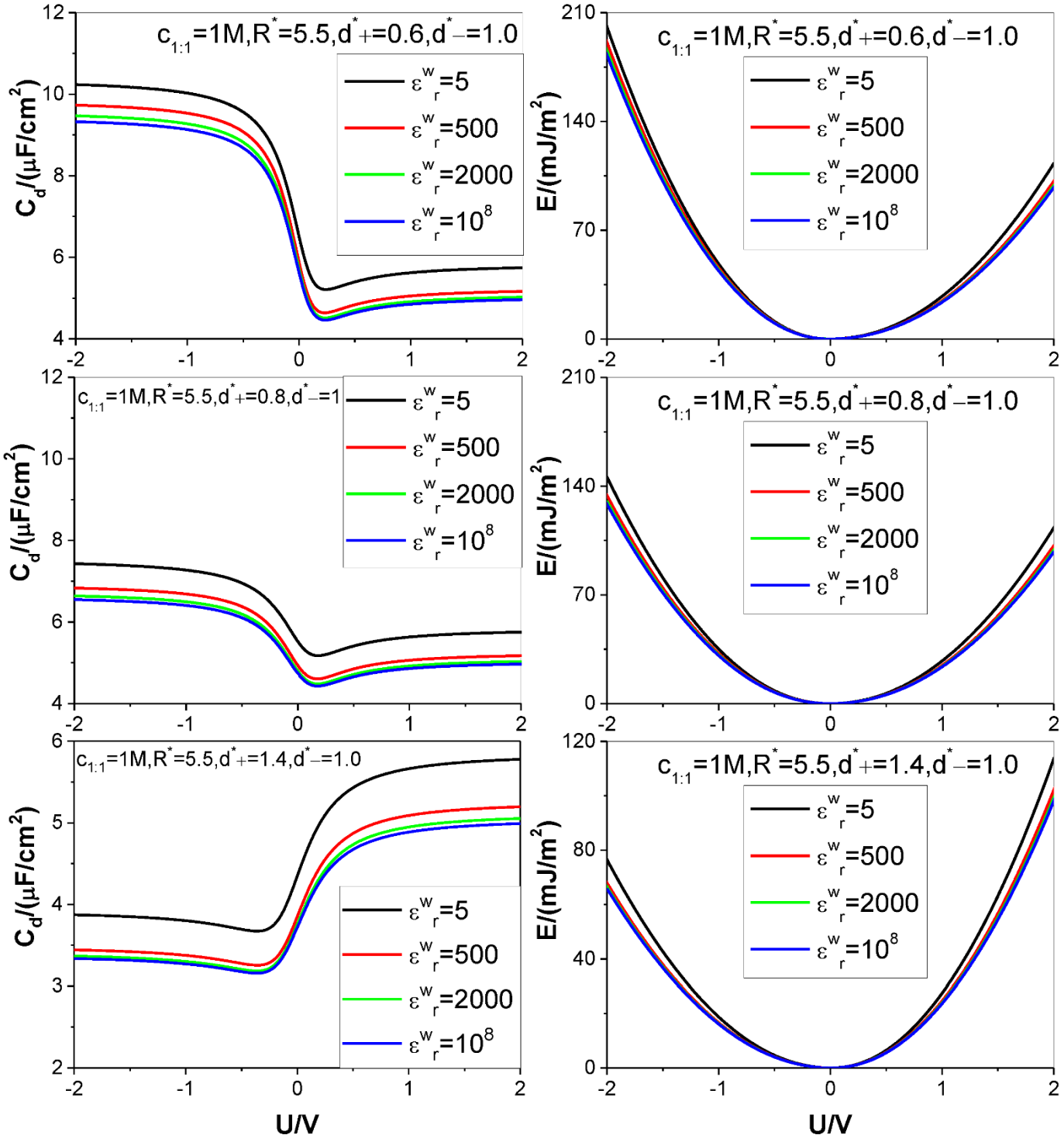

Figure 4. Same as in Figure 2 except that three values of diameter of cation (+1:−1 salt) are considered. Values of other parameters are marked in the text and figures, respectively.

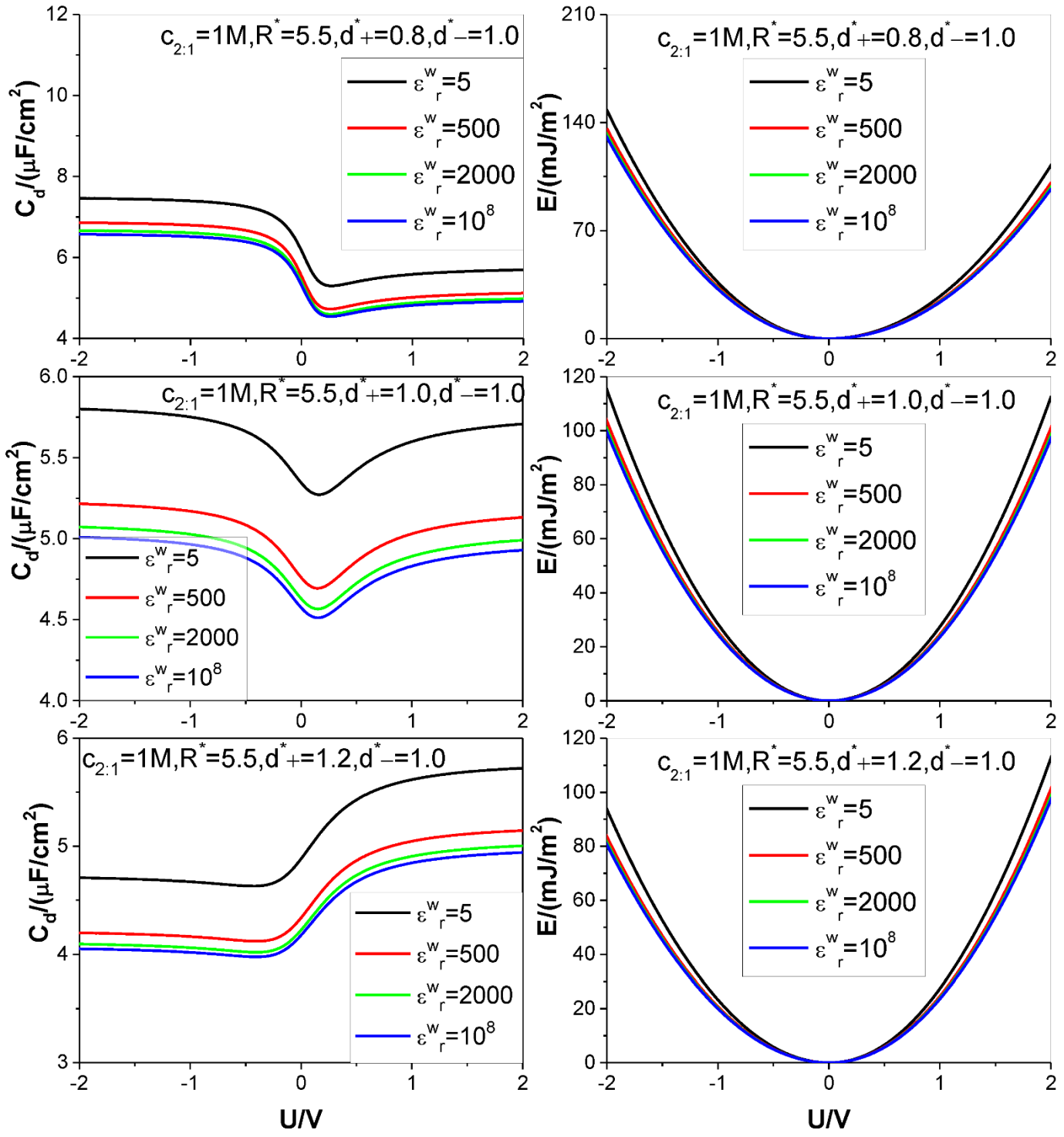

Figure 5. Same as in Figure 2 except that three values of diameter of cation (+2:−1 salt) are considered. Values of other parameters are marked in the text and figures, respectively.

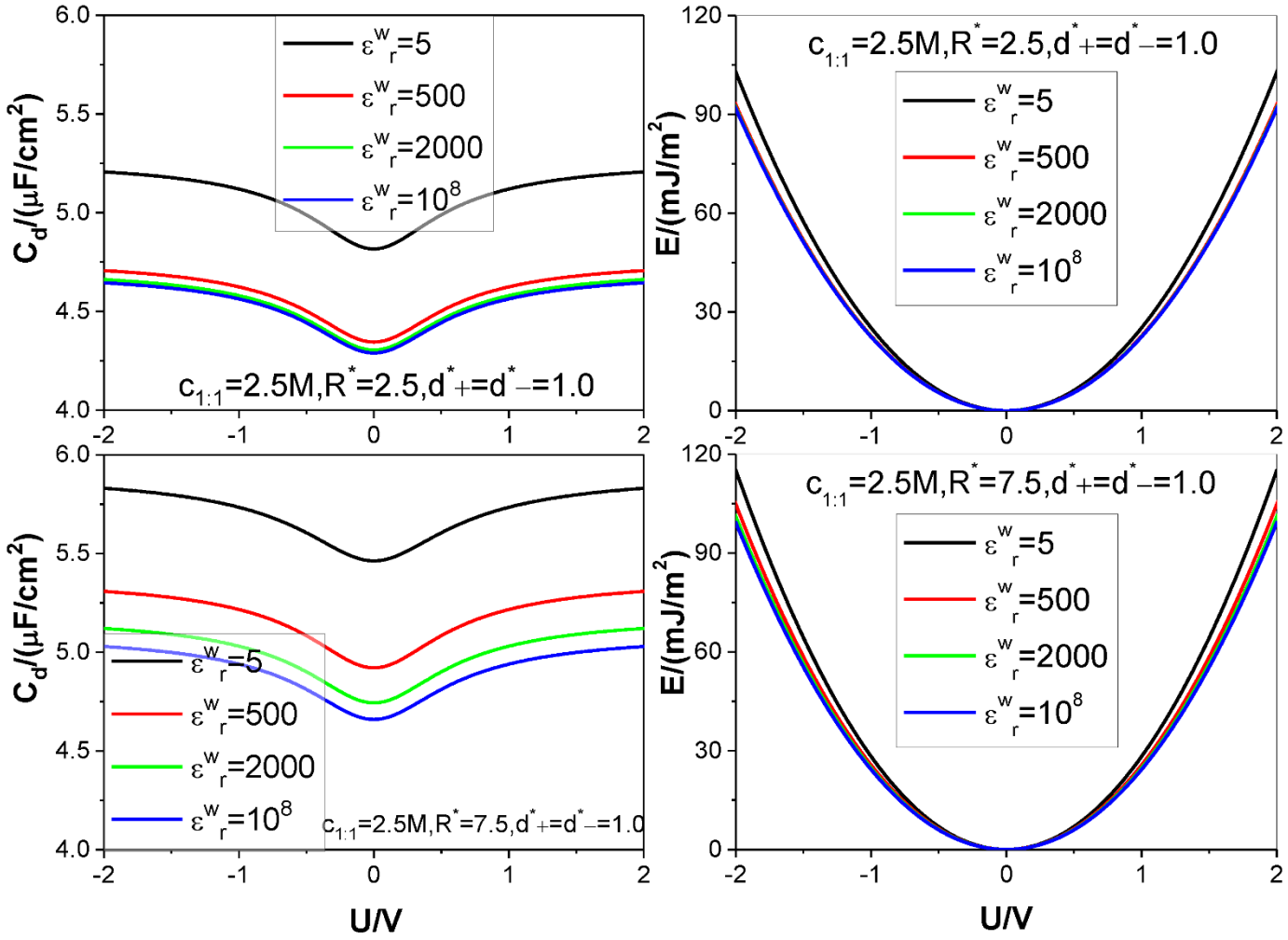

Figure 6. Same as in Figure 2 except that two values of reduced pore radius R^* are considered. Values of other parameters are marked in the text and figures, respectively.

Table 1. Summary of studied parameters.

Figure No	c/mol L^{-1}	ε_r^w	R/d	d^+/d	d^-/d	m:n	T/K	ε_r
Figure 2	1.0 2.5 4.0	5, 500, 2000, 10^8	4.5	1	1	1:1	298.15	10
Figure 3	0.125 2.0 4.0	5, 500, 2000, 10^8	5.5	1	1	2:1	298.15	10
Figure 4	1.0	5, 500, 2000, 10^8	5.5	0.6 0.8 1.4	1	1:1	298.15	10
Figure 5	1.0	5, 500, 2000, 10^8	5.5	0.8 1.0 1.2	1	2:1	298.15	10
Figure 6	2.5	5, 500, 2000, 10^8	2.5 7.5	1	1	1:1	298.15	10

The calculation results for the SC specific differential capacitance C_d and specific energy storage E are presented in Figures 2–6. We will summarize the outcomes caused by

the low solution ε_r value and different values of the electrode relative dielectric constant ε_r^w by giving a detailed analysis on the present results and comparing the present results with those based on bulk aqueous ε_r value, as published previously. To support the analysis, we present in Figures 7 and 8 the co- and counter-ion adsorption curves and electrostatic potential profiles within the pore for several parameter combinations in Table 1.

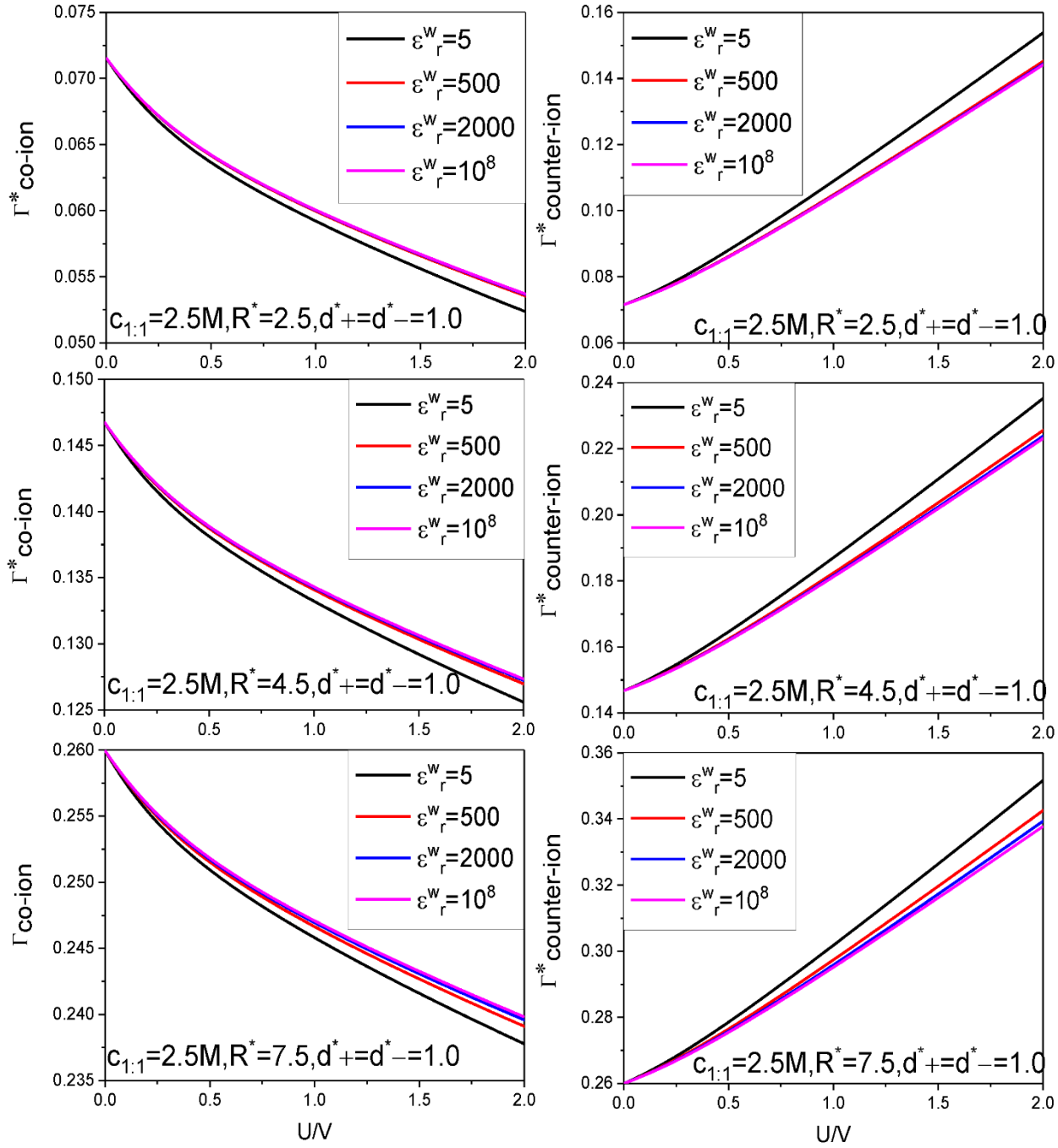

Figure 7. Co-ion and counter-ion adsorption capacities as a function of electrode surface potential. Three cylindrical pore radii and four values of the electrode surface relative dielectric constant are considered. Values of other parameters are marked in the figure.

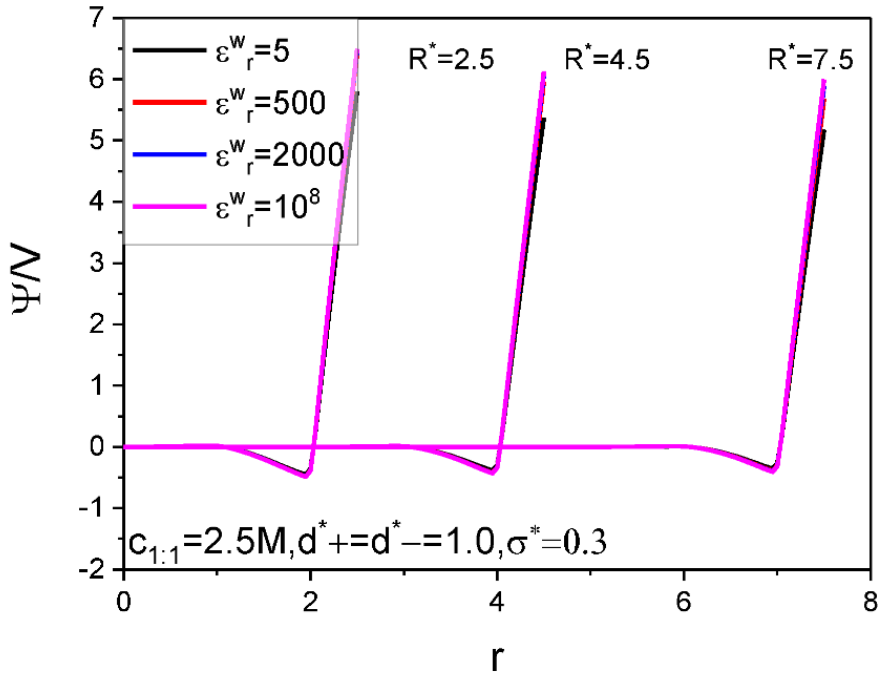

Figure 8. Electrostatic potential profiles within the pore with three different pore radii. The reduced electrode surface charge density is fixed as $\sigma^* = 0.3$, and four values of the electrode surface relative dielectric constant are considered. Values of other system parameters are marked in the figure.

One of the most significant changes caused by the low ε_r value is that both the E value and the C_d value reduce greatly with the low ε_r value dropping. Generally speaking, previous studies indicate repeatedly [73,74] that the C_d value falls within order of magnitude of F/m^2 for the normal aqueous ε_r value, such as $\varepsilon_r = 78.5$, whereas for the low ε_r value, as considered presently, such as $\varepsilon_r = 10$, the C_d value falls within order of magnitude of $\mu F/cm^2$. i.e., the C_d value goes down two orders of magnitude for approximately equal electrode potential. Corresponding to this, the E value at voltage of 2 V reduces to one twentieth of the E value corresponding to $\varepsilon_r = 78.5$ [73]. We will explore the relevant action mechanisms by analyzing the ion adsorption inside the pore and the space electrical potential distribution. The principle of electrostatic field points out that strength of the electrical potential generated by a point charge is in inverse proportion to the medium ε_r value. Given equal ion distribution profile and surface charge distribution the electrical potential strength will increase with dropping of the medium ε_r value. As a result, the curve of the voltage versus surface charge becomes less steep; the C_d value and E value reduce accordingly. On the other hand, with decreasing of the solution medium ε_r value, inter-ionic electrostatic interaction strength increases. Considering that the counter-ions dominate the pore unless around a zero charge potential (ZCP), on the average, the inter-counter-ion electrostatic interaction gets more and more repulsive with decrease of the ε_r value. As a result, the inter-counter-ion average separation tends to enlarge to lower the system energy; moreover, the effect increases with decrease of the ε_r value. Consequently, the counter-ion adsorption capacity is lower in $\varepsilon_r = 10.0$ than in $\varepsilon_r = 78.5$, and from the point of ion-filling, both the C_d and E values necessarily reduce with the decrease of the ε_r value, as it is.

It is noted that the bulk mole concentration influence is far smaller in $\varepsilon_r = 10.0$ than in $\varepsilon_r = 78.5$. The weakening of the influence is reflected in two aspects. First, compared with the $U - C_d$ curves for $\varepsilon_r = 78.5$, which change from the camel-shaped to bell-shaped with the bulk concentration changing from 1 M to 4 M, it is difficult for the $U - C_d$ curves with $\varepsilon_r = 10.0$ to finish the shape transition over the same concentration range. However, the trend of the $U - C_d$ curve shape transition is the same, i.e., with the bulk concentration increasing, the well depth of the camel-shaped curve around the ZCP gets shallower

and shallower, and the shape transition trend will eventually emerge. The reason why concentration induces the transition from camel shaped curve to bell shaped curve near ZCP is that concentration is an adsorption driving force. Even if there is no electric field potential energy, enough ions can be adsorbed near the electrode by bulk concentration alone, so that a capacitance peak appears near the ZCP. Now, due to the relatively low dielectric constant value used in the calculation, it undoubtedly increases the Coulomb repulsion energy between the adsorbed ions, thus reducing the amount of ion adsorption near the ZCP, making it difficult for the peak capacitance to appear. Second, influence of the bulk concentration on the $U - E$ curve is almost unobserved. This is not in contradiction with the $U - C_d$ curve concentration dependence. The $U - C_d$ curve change caused by the bulk concentration is mainly around the ZCP, as shown in the Figures 2 and 3; as a result, the C_d change with the bulk concentration does not cause obvious change of the integrand function in the integral in Equation (9). So, the influence of the $C_d - U$ curve change does not cause obvious change of the $U - E$ curve, as it is. Both the bulk concentration and the voltage serve as driving force for the ion adsorption. Because the low ε_r value strengths the electrostatic interaction between the surface charge and the ion, the bulk concentration influence is necessarily weakened. It is observed from Figure 3 that the $C_d - U$ curve is no longer symmetrical around the zero potential point, this is due to the ion electric valence asymmetry. However, the minimum of the C_d does not occur at U = 0 V. From the Figure 3, the minimum potential moves to certain positive potential without exception, this is obviously related to the electric valence difference. When the bulk mole concentration is very low, the adsorption capacity is very low at the zero charge potential because the driving force coming from the concentration difference is very low. As a result of the very low adsorption capacity, the electric valence asymmetry effect cannot be displayed, the C_d minimum still occurs at U = 0 V. With increasing of the bulk mole concentration, the driving force from the concentration difference increases; correspondingly, the adsorption capacity at zero charge potential is no longer negligible, and well depth of the $C_d - U$ curve reduces [81]. At very close to the zero charge potential, also because of the non-negligibility of the adsorption capacity, the electric valence asymmetry effect is displayed more and more obviously. Because the anion charge strength is lower than the cation one, at positive potential electrode, whose counter-ion is anion, the relevant C_d value is necessarily lower than that at negative potential electrode. The final outcome is that the C_d minimum occurs at an appropriate positive potential electrode.

For asymmetrical electrolytes, such as those with ion valency or ion size asymmetries, both the $U - C_d$ and $U - E$ curves become asymmetrical w.r.t. the ZCP, as expected. In detail, higher ion valency and/or smaller ion size help(s) in raising the C_d and E values whether the bulk relative dielectric constant $\varepsilon_r = 10$ or $\varepsilon_r = 78.5$. The main difference is that the counter-ion valency effect in $\varepsilon_r = 10$ becomes far less obvious than when it is in $\varepsilon_r = 78.5$. As a result, the curve asymmetry caused by the valency asymmetry is not so obvious, as when in $\varepsilon_r = 78.5$. The difference originates from a balance between two factors working in opposite directions. On one hand, the counter-ion of higher valency will increase the charge storage given the same ion adsorption capacity. On the other hand, high electrical valency helps in raising the inter-counter-ion electrostatic repulsion, and this tends to decrease the ion adsorption capacity and accordingly the charge storage; moreover, the trend is reinforced by the low bulk ε_r value. As a result, of the two factors, the one restraining the increasing of the charge storage can show its effect better in $\varepsilon_r = 10$ than in $\varepsilon_r = 78.5$. However, one may ask: why the counter-ion size effect remains significant enough in $\varepsilon_r = 10$? It is well-known that the hard sphere repulsion is an interaction far stronger than the electrostatic interaction; as a result, change of the latter strength caused by the lowering of the ε_r value, is far weaker than that caused by the former.

For aqueous component electrolyte solution, the electrolysis will occur at the electrode once a voltage of approximately 1.25 V is applied. However, recent effort succeeds in expanding the electrochemical window of aqueous electrolytes [82]. Moreover, by increasing hydrophobicity of the ion component by using ionic liquid or molten salt, the

electrochemical window can become wider. Molten salt and some of the ionic liquids also can be modelled by the PM. Although these nonaqueous electrolyte systems have lower relative dielectric constant, the present calculations are performed with low relative dielectric constant. So, considering the limitations caused by the convergence of algorithm used, the present calculations are performed over a range of the voltage from −2.0 V to 2.0 V. From Figures 2–6, one knows that at the maximum voltage considered the C_d value is far from approaching zero, and the E value is far from saturation, and actually is still on the rise. As a result, it is confirmed that a low ε_r value significantly increases the saturation voltage, beyond which the E value does not further increase with the voltage applied. The essential reason for the above phenomenon is that the low ε_r value strengths the inter-ionic electrostatic interaction, and accordingly the electrostatic repulsion between the counter-ions, the dominating ions in the pore, increases. Consequently, to keep the counter-ions accommodated in the pore in an energetically favorable way, a higher voltage is needed to offset the electrostatic repulsion between the counter-ions by the electrostatic attraction between the surface charge and the counter-ions. Although a gentle $U - \sigma$ curve always enables a small value of the C_d, it causes a higher value of the voltage corresponding to the pore closely packed state, as analyzed above. It is known that the energy storage is roughly proportional to square of the voltage, but only proportional to the C_d value; so, the high value of the saturation voltage caused by the low ε_r value significantly increases the saturation E value. However, to make high voltage value practically possible, one must use suitable nonaqueous electrolyte with a wider voltage window. Usually, hydrophobic ionic liquids are of a stable electrochemical window up to 6 V. In fact, the ionic liquids are usually free of polar solvent, value of the relevant ε_r is probably even lower than the present $\varepsilon_r = 10$ to be responsible for accounting for the electronic polarization of the ions.

It is found that with the decreasing of the electrode ε_r^w value, both the C_d and E values rise monotonously for all voltages considered. Generally speaking, for voltage strength of 2 V, an E value increase rate of 15% can be achieved by reducing the ε_r^w value from 10^8 corresponding to a metal electrode to 5 corresponding to a dielectric electrode. It should be pointed out that the electrode surface is covered with electrolyte, the electrode material largely affects the transfer of charge. So, the 15% increase rate is obtained at the cost of slowed dynamic process. However, two points analyzed below make one believe that decreasing the electrode ε_r^w value is still an effective way to improve synthetic performance of the SC. First, obviously, from the changing trend of the $U - E$ curves, one can expect that the E increase rate will rise even faster with the voltage. Considering that a high saturation voltage value is always associated with the low ε_r value electrolyte, and the relevant stable electrochemical window for some ionic liquids can be up to 6 V, as analyzed above, the E value increase rate far higher than 15% can be achieved. Second, exactly, use of the dielectric electrode may slow down the relevant dynamic process; so it is necessary to strike a balance between the energy storage density and power density of the SC. Fortunately, use of the SC is partially encouraged by its exceptionally high power density and fast charging and low effective series resistance, so there is room to move the balance point to be favorable for the E value increase rate. Further work is needed to determine the optimal parameter combination to solve this dilemma. As for why a low electrode ε_r^w value always causes both the C_d and E to rise, it can be analyzed from the perspective of dielectric polarization. With a given σ value, the higher the ε_r^w value is, the more intense the electric polarization vector **P** caused. According to formula: $|\sigma'| = |P_n|$ (P_n is the normal component of **P**), the bound charge area density strength $|\sigma'|$ rises with the ε_r^w value. Consequence of this correlation is that more co-ions can be accumulated near the electrode surface, and at the same time, the counter-ion adsorption in the vicinity of the electrode drops somewhat because the counter-ions are repelled by the likely charged bound charges when they approach the interface, and the presence of the co-ion at the electrode surface leaves less space for the counter-ion to stay there. The two changes work in the same direction and help in raising the surface electric potential strength. On the other hand, the sign of the bound charge is always opposite to that of the electrode surface

charge, so presence of the bound charge always tends to reduce the surface electric potential strength. However, the double effects occurring inside of the pore overpasses the single effect occurring outside of the pore, so the net effect is that the surface electric potential strength increases with the ε_r^w value under circumstance of fixed σ value, and accordingly, both the C_d and E values drop with the ε_r^w value, as it is. Figure 7 clearly shows the positive correlation between the co-ion adsorption and the ε_r^w value and the negative correlation between the counter-ion adsorption and ε_r^w value.

Figure 6 displays the pore size effect on the differential capacitance and energy storage. It is shown that the $U - C_d$ curves move up as a whole with the R value. It is known that a larger pore is always associated with a smaller curvature, which makes for easy gathering of the counter-ion around the electrode surface; this necessarily contributes to reduce the surface electrical potential strength, as clearly shown in Figure 8, and increase the electrical capacitance, as it is. The E value is positively correlated with the pore size. This is expected because the larger the pore size, the more the ions can be accommodated; with increasing of the voltage, more and more co-ions are excluded out of the near electrode region, instead, more counter-ions are adsorbed, as shown in Figure 7. Consequently, inter-counter-ion electrostatic repulsions play an increasingly important role; moreover, the repulsions are strengthened by the low ε_r value. As a result, the pore size effect is not as big as expected as the enhanced repulsions between the counter-ions enlarge the inter-counter-ion separation and accordingly reduce the pore space utilization and the counter-ion adsorption capacity. With further increase of the voltage applied, the electrostatic attraction between electrode surface and the counter-ions increases and this helps in offsetting partially the inter-counter-ion electrostatic repulsions and making the inter-counter-ion separation reduce and the counter-ion adsorption increase. Consequently, the pore size effect on the E value gets more and more significant with the voltage for low ε_r value. It is also shown that the strength of the ε_r^w value effect is closely related with the pore size; particularly, the ε_r^w value effect gets eventually unobservable for small enough pore if the ε_r^w value differs from that corresponding to the dielectric electrode. This is expected because the electrostatic attraction between the electrode surface and the counter-ions is so strong in small size pore that the counter-ions can be closely packed regardless of the ε_r^w value. As a result, even if the ε_r^w value changes very much, the counter-ion absorption does not change to the same extent, and so do both the C_d and E, as it is.

We have not found literatures that provide the correlation of $C_d - U$ and $E - U$ curves and electrode dielectric constant. Usually, the electrode material is made of metal. With the progress of electrode manufacturing technology, electrodes mixed with non-metallic materials and with adjustable dielectric constant will become more and more common. Our data show the negative correlation between the electrode dielectric constant and the energy storage of the SC and other concomitant effects. So, the electrode dielectric discontinuity certainly elicits new changes of multiple dilemmas such as energy-power-size-hysteresis; [83] solving these dilemmas will be new growth point of the SC field.

4. Summary

The present treatment about the dielectric discontinuity is rather general and applies for any version of the CDFT as we account for the dielectric discontinuity issue by solving numerically the boundary value problem of the Poisson equation. We employ the PM for the electrolyte solution with a relative dielectric constant ε_r being fixed at 10.0, far smaller than that of the bulk water, to reflect the actual situation of extremely small size pore. Consequently, the present results are of practical significance. The main conclusions are summarized as follows.

(i) The low solution ε_r value greatly reduces both the C_d value and the E value under certain electrode potential, but at the same time, significantly increases the saturation voltage, beyond which the E value does not further increase with the voltage applied, which significantly increases the saturation E value because of the approximate pro-

portional relation between the energy storage and square of the voltage in comparison to the proportional relation between the energy storage and the C_d value.

(ii) Because of the low solution ε_r value, influence of electrolyte bulk concentration on C_d is rather small except when the electrode potential is around the ZCP; consequently, the energy storage curves are rather insensitive to the electrolyte bulk concentration.

(iii) Higher counter-ion valency or smaller counter-ion size help in raising the C_d and E values. The enhancing effect of the counter-ion valency reduces greatly with dropping of the ε_r value; whereas the counter-ion size effect remains significant enough for low ε_r value.

(iv) Both the C_d and E values increase monotonously with the electrode dielectric constant ε_r^w decreasing for all voltages considered; the E increase rate with the dropping of the ε_r^w value rises faster with the voltages, and for voltage strength of 2 V the E value increase rate up to 15% can be achieved by reducing the ε_r^w value from 10^8 to 5. For small enough pore the ε_r^w value effect gets unobservable when the ε_r^w value differs from that corresponding to dielectric electrode.

(v) Both the C_d and the E values are positively correlated with the pore size; but for the low ε_r value considered the pore size effect on the E value gets more and more significant with the voltage applied.

Funding: This research was financially supported by National Natural Science Foundation of China (Grants 22173117).

Institutional Review Board Statement: Not applicable.

Informed Consent Statement: Not applicable.

Data Availability Statement: The data that support the findings of this study are available from the corresponding author upon reasonable request.

Acknowledgments: This project is supported by the National Natural Science Foundation of China (Grants 22173117). This work is supported in part by the High Performance Computing Center of Central South University.

Conflicts of Interest: The author declares no conflict of interest.

References

1. Rogers, W.B. A mean-field model of linker-mediated colloidal interactions. *J. Chem. Phys.* **2020**, *153*, 124901. [CrossRef] [PubMed]
2. Carrique, F.; Ruiz-Reina, E.; Arroyo, F.J.; Delgado, A.V. Influence of ion size effects on the electrokinetics of aqueous salt-free colloids in alternating electric fields. *Phys. Rev. E* **2020**, *102*, 032614. [CrossRef] [PubMed]
3. Duan, C.; Li, W.; Wang, R. Conformation of a single polyelectrolyte in poor solvents. *J. Chem. Phys.* **2020**, *153*, 064901. [CrossRef] [PubMed]
4. Nikam, R.; Xu, X.; Kanduč, M.; Dzubiella, J. Competitive sorption of monovalent and divalent ions by highly charged globular macromolecules. *J. Chem. Phys.* **2020**, *153*, 044904. [CrossRef]
5. Semenyuk, P.I.; Efimova, A.A.; Lentin, I.I.; Le-Deygen, I.M.; Izumrudov, V.A. Interaction of Ionenes with Lipid Membrane: Unusual Impact of Charge Density. *Langmuir* **2020**, *36*, 14717–14727. [CrossRef]
6. Shen, G.; Sun, Y.; Wang, Y.; Lu, X.; Ji, X. Interfacial structure and differential capacitance of ionic liquid/graphite interface: A perturbed-chain SAFT density functional theory study. *J. Mol. Liq.* **2020**, *310*, 113199. [CrossRef]
7. Heo, M.; Shin, G.R.; Kim, S.-C. Capacitance of electrolytes with hydration-mediated interaction in planar electric double layers. *Mol. Phys.* **2019**, *118*, e1610196. [CrossRef]
8. Chenn, I.; Sigal, I.M. On Derivation of the Poisson–Boltzmann Equation. *J. Stat. Phys.* **2020**, *180*, 954–1001. [CrossRef]
9. Antonova, A.; Barbero, G.; Evangelista, L.R.; Tilli, P. Ambipolar diffusion in the low frequency impedance response of electrolytic cells. *J. Stat. Mech. Theory Exp.* **2020**, *2020*, 043202. [CrossRef]
10. Razmkhah, M. Effects of carboxylic group on bulk and electrical double layer properties of amino acid ionic liquid. *J. Mol. Liq.* **2019**, *299*, 112158. [CrossRef]
11. Elisea-Espinoza, J.J.; González-Tovar, E.; Martínez-González, J.A.; Peña, C.G.G.; Guerrero-García, G.I. On the non-dominance of counterions in the 1:z planar electrical double layer of point-ions. *Mol. Phys.* **2021**, *119*. [CrossRef]
12. Arun, L.; Karthikeyan, C.; Philip, D.; Unni, C. Optical, magnetic, electrical, and chemo-catalytic properties of bio-synthesized CuO/NiO nanocomposites. *J. Phys. Chem. Solids* **2020**, *136*, 109155. [CrossRef]

13. Zhao, R.; Remsing, R.C.; Weeks, J.D. Response Theory for Static and Dynamic Solvation of Ionic and Dipolar Solutes in Water. *J. Stat. Phys.* **2020**, *180*, 721–738. [CrossRef]
14. Li, D.-D.; Yang, Y.-R.; Wang, X.-D.; Feng, G. Electrical Double Layer of Linear Tricationic Ionic Liquids at Graphite Electrode. *J. Phys. Chem. C* **2020**, *124*, 15723–15729. [CrossRef]
15. Šamaj, L. Attraction of Like-Charged Walls with Counterions Only: Exact Results for the 2D Cylinder Geometry. *J. Stat. Phys.* **2020**, *181*, 1699–1729. [CrossRef]
16. Gupta, A.; Rajan, A.G.; Carter, E.A.; Stone, H.A. Thermodynamics of Electrical Double Layers with Electrostatic Correlations. mboxemphJ. Phys. Chem. C **2020**, *124*, 26830–26842. [CrossRef]
17. Šamaj, L. Short-Distance Symmetry of Pair Correlations in Two-Dimensional Jellium. *J. Stat. Phys.* **2019**, *178*, 247–264. [CrossRef]
18. Khademi, M.; Barz, D.P.J. Structure of the Electrical Double Layer Revisited: Electrode Capacitance in Aqueous Solutions. *Langmuir* **2020**, *36*, 4250–4260. [CrossRef]
19. Wickramaarachchi, K.; Minakshi, M.; Aravindh, S.A.; Dabare, R.; Gao, X.; Jiang, Z.-T.; Wong, K.W. Repurposing N-Doped Grape Marc for the Fabrication of Supercapacitors with Theoretical and Machine Learning Models. *Nanomaterials* **2022**, *12*, 1847. [CrossRef]
20. Sharma, P.; Singh, D.; Minakshi, M.; Quadsia, S.; Ahuja, R. Activation-Induced Surface Modulation of Biowaste-Derived Hierarchical Porous Carbon for Supercapacitors. *ChemPlusChem* **2022**, *87*, e202200126. [CrossRef]
21. Reščič, J.; Linse, P. Potential of mean force between charged colloids: Effect of dielectric discontinuities. *J. Chem. Phys.* **2008**, *129*, 114505. [CrossRef] [PubMed]
22. Seijo, M.; Pohl, M.; Ulrich, S.; Stoll, S. Dielectric discontinuity effects on the adsorption of a linear polyelectrolyte at the surface of a neutral nanoparticle. *J. Chem. Phys.* **2009**, *131*, 174704. [CrossRef] [PubMed]
23. Markovich, T.; Andelman, D.; Orland, H. Ionic profiles close to dielectric discontinuities: Specific ion-surface interactions. *J. Chem. Phys.* **2016**, *145*, 134704. [CrossRef] [PubMed]
24. Wu, H.; Li, H.; Solis, F.J.; de la Cruz, M.O.; Luijten, E. Asymmetric electrolytes near structured dielectric interfaces. *J. Chem. Phys.* **2018**, *149*, 164701. [CrossRef]
25. Abdelaal, M.; Hung, T.-C.; Mohamed, S.; Yang, C.-C.; Huang, H.-P.; Hung, T.-F. A Comparative Study of the Influence of Nitrogen Content and Structural Characteristics of NiS/Nitrogen-Doped Carbon Nanocomposites on Capacitive Performances in Alkaline Medium. *Nanomaterials* **2021**, *11*, 1867. [CrossRef]
26. Wannasen, L.; Mongkolthanaruk, W.; Swatsitang, E.; Pavasant, P.; Pinitsoontorn, S. Co2P2O7 Microplate/Bacterial Cellulose-Derived Carbon Nanofiber Composites with Enhanced Electrochemical Performance. *Nanomaterials* **2021**, *11*, 2015. [CrossRef]
27. Zhou, S.; Zhou, R.; Tian, C. Impacts of solvent electric dipole and ion valency on energy storage in ultrananoporous supercapacitor: An ising model study. *J. Phys. Chem. Solids* **2021**, *157*, 110188. [CrossRef]
28. Zhou, S.; Zhou, R. Ising model study on effects of solvent electric dipole on ultrananoporous supercapacitor. *Chin. J. Phys.* **2021**, *73*, 391–405. [CrossRef]
29. Tergolina, V.B.; dos Santos, A.P. Effect of dielectric discontinuity on a spherical polyelectrolyte brush. *J. Chem. Phys.* **2017**, *147*, 114103. [CrossRef]
30. Guerrero García, G.I.; Olvera de la Cruz, M. Polarization Effects of Dielectric Nanoparticles in Aqueous Charge-Asymmetric Electrolytes. *J. Phys. Chem. B* **2014**, *118*, 8854–8862. [CrossRef]
31. Korobko, A.V.; Marques, C.M.; Schöps, M.; Schädler, V.; Wiesner, U.; Mendes, E. Dielectric discontinuity in equilibrium block copolymer micelles. *Soft Matter* **2015**, *11*, 7081–7085. [CrossRef] [PubMed]
32. Dos Santos, A.P.; Bakhshandeh, A.; Levin, Y. Effects of the dielectric discontinuity on the counterion distribution in a colloidal suspension. *J. Chem. Phys.* **2011**, *135*, 044124. [CrossRef] [PubMed]
33. Chen, P. Electrostatic attraction between ionic reverse micelles with dielectric discontinuity. *J. Chem. Phys.* **2002**, *117*, 9460–9464. [CrossRef]
34. Wernersson, E.; Kjellander, R. Image Charges and Dispersion Forces in Electric Double Layers: The Dependence of Wall−Wall Interactions on Salt Concentration and Surface Charge Density. *J. Phys. Chem. B* **2007**, *111*, 14279–14284. [CrossRef] [PubMed]
35. Jho, Y.S.; Park, G.; Chang, C.S.; Pincus, P.A.; Kim, M.W. Effects of dielectric discontinuities on two charged plates. *Phys. Rev. E* **2007**, *76*, 011920. [CrossRef]
36. Wernersson, E.; Kjellander, R. Ion correlation forces between uncharged dielectric walls. *J. Chem. Phys.* **2008**, *129*, 144701. [CrossRef]
37. Téllez, G.; Trizac, E. A Two-Dimensional One Component Plasma and a Test Charge: Polarization Effects and Effective Potential. *J. Stat. Phys.* **2012**, *146*, 832–849. [CrossRef]
38. Curtis, R.; Lue, L. Depletion forces due to image charges near dielectric discontinuities. *Curr. Opin. Colloid Interface Sci.* **2015**, *20*, 19–23. [CrossRef]
39. Varela, L.; Téllez, G.; Trizac, E. One-dimensional colloidal model with dielectric inhomogeneity. *Phys. Rev. E* **2021**, *103*, 042603. [CrossRef]
40. Odinaev, S.; Akdodov, D.M.; Makhmadbegov, R.S. Makhmadbegov, study of the frequency dispersion of dielectric permittivity and dielectric loss coefficient for aqueous potassium iodide solutions. *J. Struct. Chem.* **2022**, *63*, 964–975. [CrossRef]
41. Evans, R. Nature of the liquid-vapor interface and other topics in the statistical mechanics of nonuniform classical fluids. *Adv. Phys.* **1979**, *28*, 143. [CrossRef]

42. Henderson, D. (Ed.) *Fundamentals of Inhomogeneous Fluids*; Marcel Dekker: New York, NY, USA, 1992.
43. Vergara, E.L.C.; Kontogeorgis, G.M.; Liang, X. Gas Adsorption and Interfacial Tension with Classical Density Functional Theory. *Ind. Eng. Chem. Res.* **2019**, *58*, 5650–5664. [CrossRef]
44. Marshall, B.D. A theoretical analysis on the separation of mixtures by extractive adsorption. *Chem. Eng. Sci.* **2021**, *235*, 116460. [CrossRef]
45. Kolesnikov, A.L.; Budkov, Y.A.; Gor, G.Y. Adsorption-induced deformation of mesoporous materials with corrugated cylindrical pores. *J. Chem. Phys.* **2020**, *153*, 194703. [CrossRef]
46. Eller, J.; Gross, J. Free-Energy-Averaged Potentials for Adsorption in Heterogeneous Slit Pores Using PC-SAFT Classical Density Functional Theory. *Langmuir* **2021**, *37*, 3538–3549. [CrossRef] [PubMed]
47. Myhal, V.; Derzhko, O. Wetting in the presence of the electric field: The classical density functional theory study for a model system. *Phys. A Stat. Mech. Its Appl.* **2017**, *474*, 293–300. [CrossRef]
48. Zhou, S. Wetting Transition of Nonpolar Neutral Molecule System on a Neutral and Atomic Length Scale Roughness Substrate. *J. Stat. Phys.* **2018**, *170*, 979–998. [CrossRef]
49. Kundu, P.; Mishra, P.; Jaiswal, A.; Ram, J. Structures and phase transition in a two-dimensional system of Gay-Berne molecules. *J. Mol. Liq.* **2019**, *296*, 111769. [CrossRef]
50. Morfe, P.S. Surface Tension and Gamma-Convergence of Van der Waals-Cahn-Hilliard Phase Transitions in Stationary Ergodic Media. *J. Stat. Phys.* **2020**, *181*, 2225–2256. [CrossRef]
51. Gußmann, F.; Dietrich, S.; Roth, R. Toward a density-functional theory for the Jagla fluid. *Phys. Rev. E* **2020**, *102*, 062112. [CrossRef]
52. Kim, H.; Schimmele, L.; Dietrich, S. Wetting behavior of a colloidal particle trapped at a composite liquid-vapor interface of a binary liquid mixture. *Phys. Rev. E* **2021**, *103*, 042802. [CrossRef] [PubMed]
53. Mondal, A. Configuraional Entropy of a parabolic potential system: A density functional approach. *Phys. Scr.* **2020**, *96*, 025703. [CrossRef]
54. Gurin, P.; Odriozola, G.; Varga, S. Enhanced two-dimensional nematic order in slit-like pores. *New J. Phys.* **2021**, *23*, 063053. [CrossRef]
55. Forsman, J.; Nordholm, S. Polyelectrolyte Mediated Interactions in Colloidal Dispersions: Hierarchical Screening, Simulations, and a New Classical Density Functional Theory. *Langmuir* **2012**, *28*, 4069–4079. [CrossRef] [PubMed]
56. Zhou, S. Inter-surface effective electrostatic interactions in the presence of surface charge discreteness and solvent granularity. *Mol. Phys.* **2020**, *118*, e1778807. [CrossRef]
57. Zhou, S. On the statistical mechanics investigation of structure and effective electrostatic force between two solid surfaces in electrolyte dissolved in non-polar solvent. *J. Stat. Mech. Theory Exp.* **2020**, *2020*, 073210. [CrossRef]
58. Balzer, C.; Jiang, J.; Marson, R.L.; Ginzburg, V.V.; Wang, Z.-G. Nonelectrostatic Adsorption of Polyelectrolytes and Mediated Interactions between Solid Surfaces. *Langmuir* **2021**, *37*, 5483–5493. [CrossRef]
59. Haertel, A. Structure of electric double layers in capacitive systems and to what extent (classical) density functional theory describes it. *J. Phys. Condens. Mat.* **2017**, *29*, 423002. [CrossRef]
60. Faramarzi, E.; Maghari, A. The effect of dispersion interactions on the structure and performance of electrical double layer of ionic liquids. *J. Mol. Liq.* **2017**, *246*, 325–331. [CrossRef]
61. Neal, J.N.; Wesolowski, D.J.; Henderson, D.; Wu, J. Electric double layer capacitance for ionic liquids in nanoporous electrodes: Effects of pore size and ion composition. *J. Mol. Liq.* **2018**, *270*, 145–150. [CrossRef]
62. Yang, G.; Prasianakis, N.I.; Churakov, S.V. Comparative Modeling of Ions and Solvent Properties in Ca-Na Montmorillonite by Atomistic Simulations and Fluid Density Functional Theory. *Clays Clay Miner.* **2020**, *68*, 100–114. [CrossRef]
63. Yang, J.; Ding, Y.; Lian, C.; Ying, S.; Liu, H. Theoretical Insights into the Structures and Capacitive Performances of Confined Ionic Liquids. *Polymers* **2020**, *12*, 722. [CrossRef] [PubMed]
64. Jiang, J.; Ginzburg, V.V.; Wang, Z.-G. On the origin of oscillatory interactions between surfaces mediated by polyelectrolyte solution. *J. Chem. Phys.* **2019**, *151*, 214901. [CrossRef] [PubMed]
65. Vrugt, M.T.; Löwen, H.; Wittkowski, R. Classical dynamical density functional theory: From fundamentals to applications. *Adv. Phys.* **2020**, *69*, 121–247. [CrossRef]
66. Binder, K.; A Egorov, S.; Milchev, A.; Nikoubashman, A. Understanding the properties of liquid-crystalline polymers by computational modeling. *J. Phys. Mater.* **2020**, *3*, 032008. [CrossRef]
67. Lutsko, J.F.; Lam, J. Classical density functional theory, unconstrained crystallization, and polymorphic behavior. *Phys. Rev. E* **2018**, *98*, 012604. [CrossRef]
68. Somerville, W.R.C.; Stokes, J.L.; Adawi, A.M.; Horozov, T.S.; Archer, A.J.; A Buzza, D.M. Density functional theory for the crystallization of two-dimensional dipolar colloidal alloys. *J. Phys. Condens. Matter* **2018**, *30*, 405102. [CrossRef]
69. Lutsko, J.F.; Schoonen, C. Classical density-functional theory applied to the solid state. *Phys. Rev. E* **2020**, *102*, 062136. [CrossRef]
70. Ney, E.M.; Hou, C.-H.; Taboada-Serrano, P. Calculation of Electrical Double Layer Potential Profiles in Nanopores from Grand Canonical Monte Carlo Simulations. *J. Chem. Eng. Data* **2018**, *63*, 2557–2566. [CrossRef]
71. Heo, M.; Shin, G.R.; Kim, S.-C. Differential capacitance of uniformly charged hard-sphere ions in planar electric double layers. *J. Stat. Mech. Theory Exp.* **2019**, *2019*, 083207. [CrossRef]

72. Islam, S.; Lamperski, S.; Islam, M.; Henderson, D.; Bhuiyan, L.B. Temperature dependence of differential capacitance in the electric double layer.Symmetric valency 1:1 electrolytes. *J. Chem. Phys.* **2020**, *152*, 204702. [CrossRef] [PubMed]
73. Zhou, S. A statistical mechanics study on relationship between nanopore size and energy storage in supercapacitors. *J. Phys. Chem. Solids* **2020**, *148*, 109705. [CrossRef]
74. Zhou, S. Solvent granularity in the differential electrical capacitance of supercapacitor and mechanism analysis. *Phys. A Stat. Mech. Appl.* **2019**, *533*, 121905. [CrossRef]
75. Sato, T.; Sasaki, T.; Ohnuki, J.; Umezawa, K.; Takano, M. Hydrophobic Surface Enhances Electrostatic Interaction in Water. *Phys. Rev. Lett.* **2018**, *121*, 206002. [CrossRef] [PubMed]
76. Alawneh, M.; Henderson, D.; Outhwaite, C.; Bhuiyan, L. The effect of dielectric polarization of the electrode on anomalous temperature effects in the electrical double layer. *Mol. Simul.* **2008**, *34*, 501–507. [CrossRef]
77. Zhou, S.; Lamperski, S.; Zydorczak, M. Properties of a planar electric double layer under extreme conditions investigated by classical density functional theory and Monte Carlo simulations. *J. Chem. Phys.* **2014**, *141*, 64701. [CrossRef]
78. Zhou, S.; Lamperski, S.; Sokołowska, M. Classical density functional theory and Monte Carlo simulation study of electric double layer in the vicinity of a cylindrical electrode. *J. Stat. Mech. Theory Exp.* **2017**, *2017*, 073207. [CrossRef]
79. Lamperski, S.; Zhou, S. Structural and electrical properties of an electric double layer formed inside a cylindrical pore investigated by Monte Carlo and classical density functional theory. *Microfluid. Nanofluid.* **2019**, *23*, 20. [CrossRef]
80. Zhou, S.; Lamperski, S. Unusual properties of the electric double layer in an extremely narrow nanotube. A grand canonical Monte Carlo and classical DFT study. *J. Phys. Chem. Solids* **2021**, *161*, 110440. [CrossRef]
81. Zhou, S. Capacitance of electrical double layer formed inside a single infinitely long cylindrical pore. *J. Stat. Mech. Theory Exp.* **2018**, *2018*, 103203. [CrossRef]
82. Yang, C.; Chen, J.; Qing, T.; Fan, X.; Sun, W.; von Cresce, A.; Ding, M.S.; Borodin, O.; Vatamanu, J.; Schroeder, M.; et al. 4.0 V Aqueous Li-Ion Batteries. *Joule* **2017**, *1*, 122–132. [CrossRef]
83. Lee, A.A.; Vella, D.; Goriely, A.; Kondrat, S. Capacitance-Power-Hysteresis Trilemma in Nanoporous Supercapacitors. *Phys. Rev. X* **2016**, *6*, 021034. [CrossRef]